Theoretical and Applied Mechanics Letters 12 (2022) 100314

Contents lists available at ScienceDirect

Theoretical and Applied Mechanics Letters

journal homepage: www.elsevier.com/locate/taml

Letter

How far the wake of a wind farm can persist for?

Guodan Dong[a,b], Zhaobin Li[a,b], Jianhua Qin[a,b], Xiaolei Yang[a,b,*]

[a] The State Key Laboratory of Nonlinear Mechanics, Institute of Mechanics, Chinese Academy of Sciences, Beijing 100190, China
[b] School of Engineering Sciences, University of Chinese Academy of Sciences, Beijing 100049, China

ARTICLE INFO

Article history:
Received 29 November 2021
Accepted 30 November 2021
Available online 21 December 2021

Keywords:
Wind farm wake
Large-eddy simulation
Actuator disk
Wind turbine wake

ABSTRACT

With the increased penetration of wind energy in our nation's energy portfolio, wind farms are placed in a way close to each other. Thus, their wakes have to be fully considered in the design and operation of a wind farm. In this study, we investigate the wake of a wind farm using large-eddy simulation with wind turbine rotor modelled by the actuator disk model. The simulated results show that the wake of a wind farm can persist for a long distance in its downstream. For the considered wind farm layout, the velocity in the wake recovers 95% of that of the undisturbed inflow at 55 rotor diameters downstream from its last row, suggesting that the wake of a wind farm should be fully considered in the optimal design and operation for its downstream wind farms.

Wind turbines are often clustered as a wind farm to extract energy from the wind. A wind farm leaves a wake in its downstream as converting wind kinetic energy into electricity, which has to be taken into account properly when designing wind farms in regions with multiple planned farms, in order to correctly estimate the annual energy production and structure loads [1]. The wake of a single wind turbine has been extensively studied in the literature [2–4]. However, investigations on the wake of a wind farm are relatively limited.

The wind farm wake, consisting of flow structures ranging from wind turbine scale (∼ 100 m) up to meteorological scale (∼ 100 km) [5], is affected by wind turbine wakes, their interaction with the atmospheric turbulence and several other factors (e.g., terrain topology, wind farm operations, and meteorologic condition) [6]. It has been shown that a wind farm wake can propagate downstream for tens of kilometers [7]. Field measurements of the Horns-Rev wind farm by satellite synthetic aperture radar [8] reveal that a speed loss of more than 2% can still be observed within a range of 5 to 20 km downstream. For the German Bight offshore wind farm, aerial measurements found that the wake speed deficit can reach up to 40% immediately downstream the wind-farm, and the wake can propagates for tens of kilometers. A nine-year long-term measurement using met tower and supervisory control and data acquisition (SCADA) data in the North sea wind farm cluster confirmed evidently that the wake of the upstream wind farm reduces the wind speed, enhances the turbulence, and increases the structural load for their downstream wind farms [9].

Besides measurements, numerical simulations with different fidelity have also been carried out in the literature. To study the regional or global effects of wind farms, the whole wind farm is often modelled as equivalent surface roughness [10] or as an elevated sink of momentum and a source of turbulent kinetic energy [11,12]. Modeling an individual turbine wake in mesoscale simulations as an elevated sink of momentum and a source of turbulent kinetic energy were also reported in the literature [13,14]. These modeling techniques without resolving wind turbine wakes allow the investigation of regional to global effects of wind farms with affordable computational resources. In the meanwhile, resolving turbine wake can provide more details of the wind-farm wake [15], which is essential for the design of wind farm layout and operation, but is more resource demanding. Most of the farm-scale simulations have been done with Reynolds-Averaged Navier-Stokes (RANS) method [16] or with large-eddy simulation (LES) utilizing a wake region less than 10 km [17,18], which is relatively short compared to the distance that the wake effect can reach as reported from measurement [8].

In this work, we present a preliminary investigation of wind farm wake with LES, to probe into the flow details of the wind farm wake. An idealized wind farm layout consisting of 40 turbines is studied in a large computational domain, allowing analyzing the wind-farm wake over 15 km long.

The turbulent flow over a wind farm is simulated using LES via the VFS-Wind code [19], in which the filtered Navier-Stokes

* Corresponding author.
E-mail address: xyang@imech.ac.cn (X. Yang).

https://doi.org/10.1016/j.taml.2021.100314

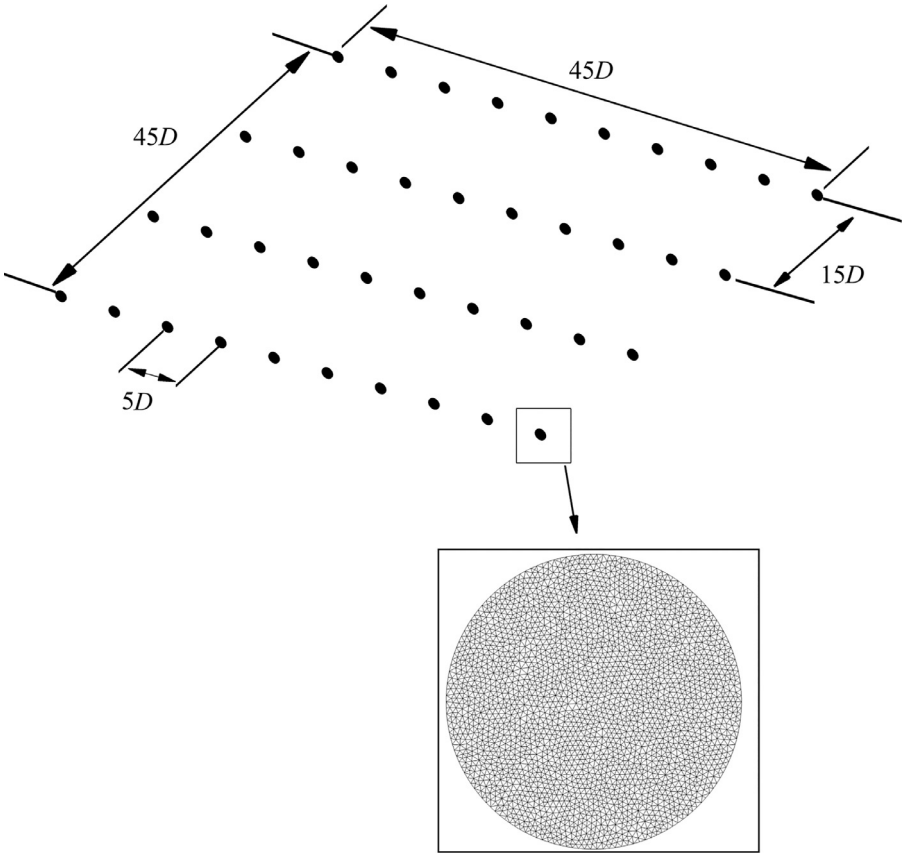

Fig. 1. Layout of the simulated wind farm and the actuator disk model for the rotor of the wind turbine.

equations for incompressible flows in the curvilinear coordinate are solved with the unresolved subgrid-scale stress modelled using the dynamic Smagorinsky model [20]. A second-order accurate central differencing scheme is employed for the spatial discretization, and the fractional step method [21] is employed for the time integration. The nonlinear momentum equation is solved with a Jacobian-Free Newton-Krylov method [22]. The Poisson equation is solved with a Generalized Minimal Residual (GMRES) method with an algebraic multigrid acceleration.

The wind turbine is parameterized by the actuator disk (AD) model with uniformly distributed axial forces [23]. The AD model, which neglects the geometry detail of individual wind turbine blades, represents the rotating blades as a fixed two-dimensional porous disk exerting a uniform thrust on the flow. In the present AD model, the axial thrust force per unit area $f_{\mathrm{T}}(t)$ is computed as follows:

$$f_{\mathrm{T}}(t) = \frac{1}{2}\rho C_{\mathrm{T}}^{'} U_{\mathrm{d}}^{2}(t), \tag{1}$$

where ρ is the density of air, U_{d} is the streamwise velocity averaged over the actuator disk, and $C_{\mathrm{T}}^{'} = 4a/(1-a)$ (where a is the axial induction factor). The above expression is derived based on the conventional definition for thrust and the one-dimensional momentum theory. The same approach has been employed in the literature for the simulation of wind farms [24,25].

As shown in Fig. 1, the simulated wind farm consists of 40 turbines arranged into 4 rows with 10 turbines in each row, and placed with the streamwise and spanwise spacings $15D$ and $5D$, respectively, in an area of an area of $45D \times 45D$, where D is the rotor diameter $D = 100$ m of the employed wind turbine with hub height $z_{\mathrm{hub}} = D$. This layout is designed using the method presented in Ref. [26] for maximizing the power output efficiency. In the simulation, the axial induction factor is fixed at $a = 0.25$ for all turbines. The employed computational domain is rectangular (as shown Fig. 2) and has a size of $L_x \times L_y \times L_z = 225D \times 148.8D \times 10D$, with x, y and z denoting the streamwise, spanwise and vertical directions, respectively. The domain is discretized by a Cartesian grid with grid nodes of $N_x \times N_y \times N_z = 1126 \times 1488 \times 152$. The grid is uniform in the x and y directions with the grid spacing $\Delta x = D/5$ and $\Delta y = D/10$. In the z direction, the grid is uniform near the ground ($z \in (0, 1.5D)$) with $\Delta z = D/50$ and is gradually stretched to the top boundary. This mesh resolution is accurate enough to capture wind turbine wake and wind farm wake according to Yang et al. [17,25].

The turbulent inflows applied at the inlet ($x = 0D$) are generated by a precursory simulation. At the outlet ($x = 225D$), Neumann boundary condition for velocity is applied. A wall model based on the logarithmic law for rough walls is applied on the ground ($u/u^* = \frac{1}{\kappa}\ln(z/z_0)$, where u^* is the friction velocity, $\kappa = 0.4$ is the Kármán constant and $z_0 = 0.001$ m is the roughness length). At the lateral and the top boundaries, the free-slip condition is applied. The time step for the simulation is $0.086D/U_{hub}$, and it take approximatly three wakes to finish this simulation (30000 steps) with 640 core on beijing super cloud computing center. The simulation runs for 4000 time steps (approximately 1.5 flowthroughs) to develop the flowfield. After that, the flowfield is averaged for 26,000 steps to compute the flow statistics.

We first show the instantaneous streamwise velocity field in Fig. 3, with zoomed-in Fig. 3b and 3c for better visualization of wind turbine wakes inside the wind farm and the near wake of the wind farm, respectively. As seen, the wake of the wind turbine is well captured in the present simulation. The flow within the farm is composed of low speed wind turbine wakes and relatively high

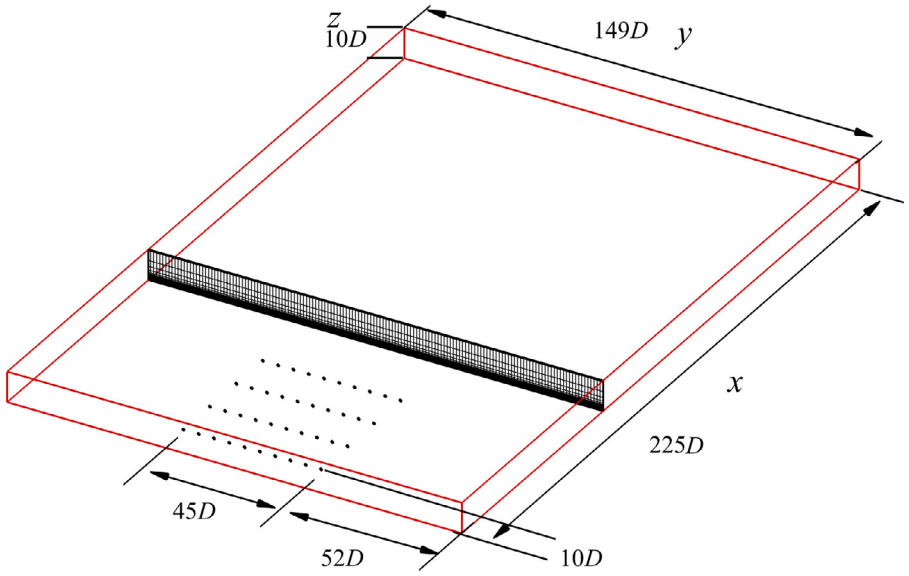

Fig. 2. Schematic of the employed computational domain. The origin "A" is indicted by a blue dot. (For interpretation of the references to colour in this figure legend, the reader is referred to the web version of this article.)

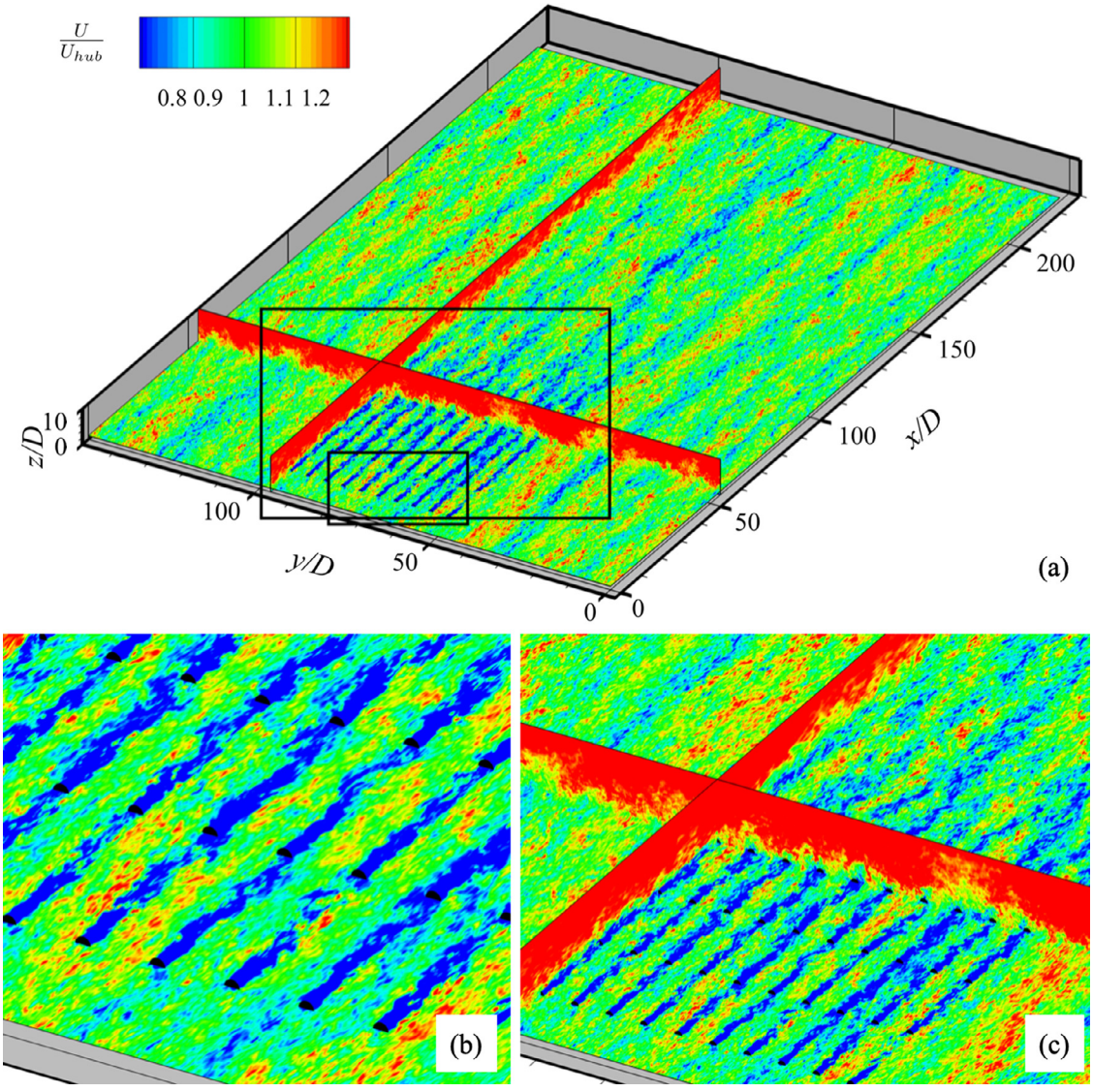

Fig. 3. (**a**) Contours of the instantaneous streamwise velocity on the $x-y$ plane at z_{hub}, $y-z$ plane at $x = 55D$ (the last row of the farm), and $z-x$ plane at $y = 96.8D$ (one of the columns along the edge of the farm). (**b**) and (**c**) Zoomed-in contours showing the turbine wake inside the wind farm and the near wake of the wind farm, respectively.

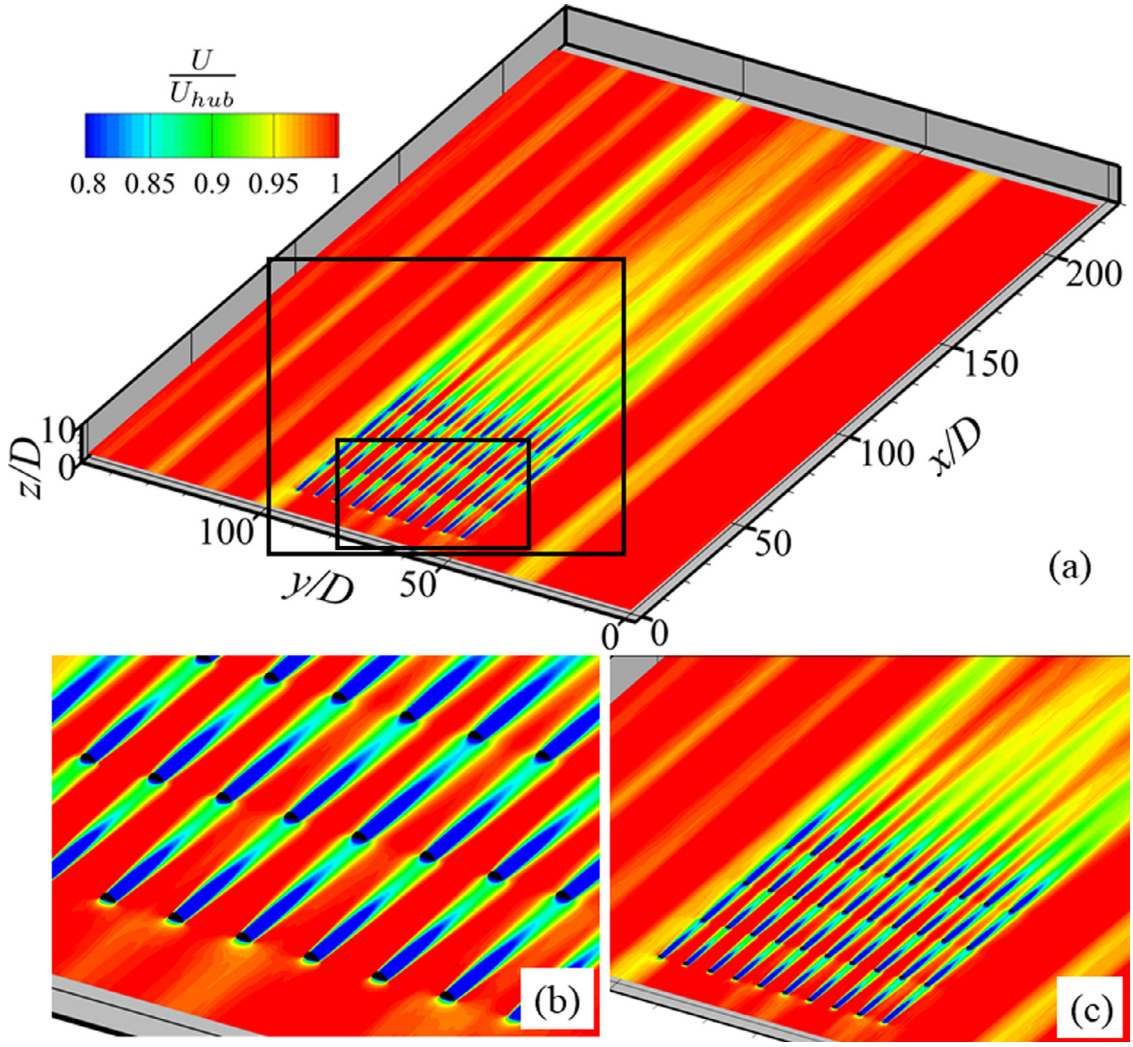

Fig. 4. (**a**) Contours of the time-averaged streamwise velocity on the $x-y$ plane at z_{hub}. (**b**) and (**c**) Zoomed-in contours showing the turbine wakes inside the farm and in near wake of the farm, respectively.

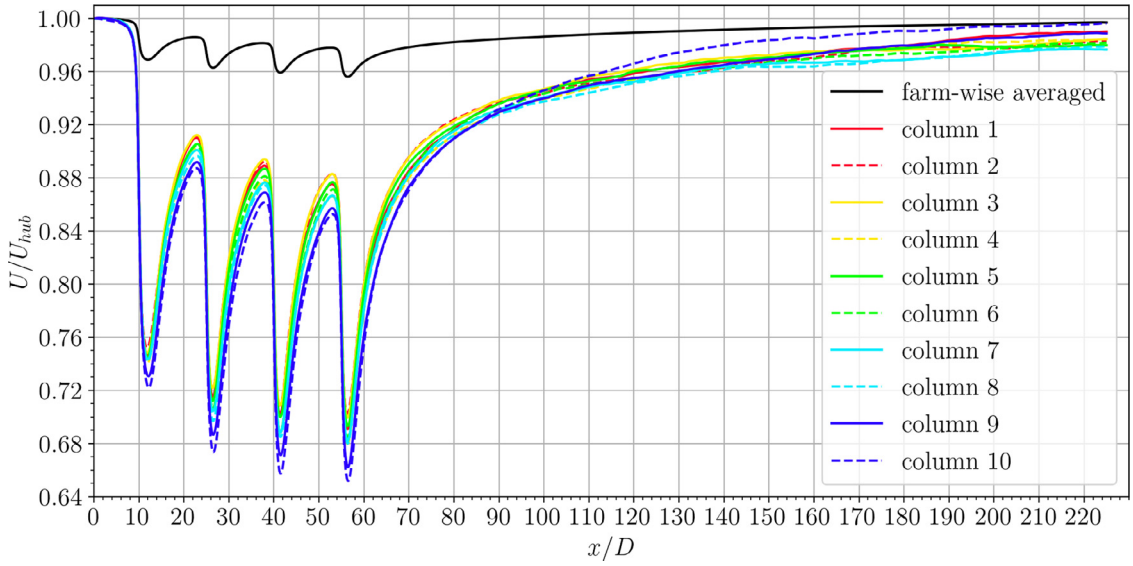

Fig. 5. Streamwise variations of spanwise-averaged streamwise velocity. Here the black solid line labelled as "farm wake averaged" corresponds to the streamwise velocity averaged from $y/D = 52$ to $y/D = 97D$ on the horizontal plane at $z = z_{hub}$. For other profiles, the streamwise velocity is averaged in the spanwise direction over a distance of D with each row of turbines in the center.

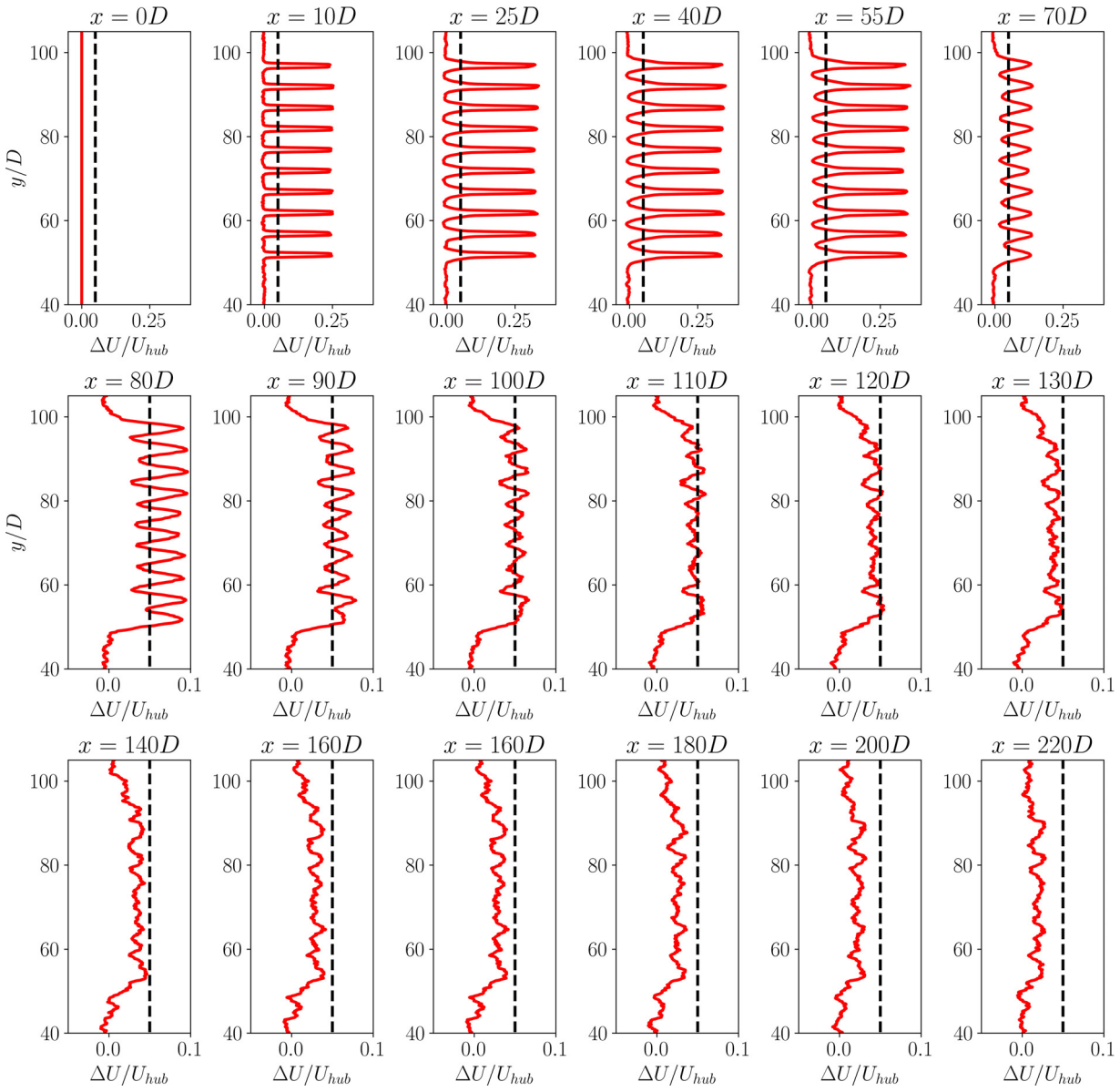

Fig. 6. Spanwise profiles of the time-averaged steamwise velocity deficit at different streamwise locations. The vertical dashed line indicates $\Delta U/U_{hub} = 0.05$ for 95 percents of wake recovery.

wind speed regions located between neighboring turbine columns. In the downstream of the farm, complex flow structures featured by the interplay of turbine wakes appear.

The time-averaged streamwise velocity field on the horizontal plane located at the hub height are then examined in Fig. 4. In the spanwise direction, the time-averaged flow field is heterogeneous because of the turbine wakes within the wind farm and the fairly complex wake of the wind farm. In general, the velocity in the wake recovers quickly to that close to U_{hub}, e.g., the one located at $y = 86.85D$and $91.85D$. However, taking the two neighboring columns of the farm located at $y = 51.85D$ and $56.85D$ for example, coalescence of the two wakes behind columns appear and the generated new wake persist for a very long distance in the downstream. In addition, the recovery of the wake will be mitigated due to the inhomogeneous inflow field in the spanwise direction, in which the low speed streaks from the inflow reinforce turbine wakes in the wind farm. Streamwise variations of the spanwise-averaged streamwise velocity are then presented in Fig. 5. Downstream variations because of turbine wakes occur for all the profiles. Figure 5 The figure indicate that the farm-wise averaged profile and wake-wise averaged profiles are different within the wind farm in its near wake. From $55D$ downstream of the last row of the wind farm, the wind farm averaged streamwise velocity is higher than 98% of U_{hub}, while those from the wake-wise averaged streamwise velocity are much lower than 98% of U_{hub}.

At last, the spanwise profiles of the streamwise velocity deficit, which is computed by subtracting the time-averaged streamwise velocity at the inlet, are shown in Fig. 6. The $10D$, $25D$, $40D$ and $55D$ are the positions of the 1–4 rows of the wind farm, respectively. The black solid line ($\Delta U = 0.05$) in the figure indicates that the velocity in the wake recovers 95% of that at the inlet. As seen, at approximately $110D$ from the inlet, i.e. $55D$ downwind of the last row of the wind farm, the velocity deficit in the wake decreases to 5% of U_{hub}. From $55D$ to $75D$ downstream of the last row, the velocity deficit, on the other hand, does not decrease significantly. As moving to further downstream locations, the velocity deficit decreases to approximately 2.5% of U_{hub} at $165D$ (which corresponds

to 16.5 km for this simulated case) downstream of the last row of the wind farm. In addition, periodic distributions of the streamwise velocity deficit are within the wind farm and the near wake of the farm propagates until 75D downstream of the last row of the wind farm. At further downstream locations, although the periodic distribution are not pronounced any more, the influences of wind turbine wakes exist even at 165D downstream of the last row of the wind farm.

In this work, we investigated the wake from a wind farm using large-eddy simulation with the rotor modelled using an actuator disk model. In the simulated wind farm, the streamwise and spanwise turbine spacings are 15D and 5D, respectively, which are designed using the method presented in Ref. [26]. The simulated results show that the streamwise velocity recovers 95% of the undisturbed incoming wind speed at 55D downstream of the last row of the wind farm. The influences of wind turbine wakes persist for a very long distance, which are still observed even at 165D downstream of the last row of the wind farm. An important suggestion from this work is that the wake from the upstream wind farm should be considered in the optimal design and control of downstream wind farms, even their distance is as far as 55D, which corresponds to 5.5 km for the simulated case.

It is noted that we considered an idealized setup for only one turbine layout. Future work will be carried out for different layouts with different turbine spacings. Factors including the Coriolis force and other atmospheric factors (e.g., thermal stratification) will also be taken into account.

Declaration of Competing Interest

The authors declare that they have no known competing financial interests or personal relationships that could have appeared to influence the work reported in this paper.

Acknowledgments

This work was supported by the National Natural Science Foundation of China (Nos. 11988102, 12172360) and Institute of Mechanics and Chinese Academy of Sciences.

References

[1] J. Lundquist, K. DuVivier, D. Kaffine, J. Tomaszewski, Costs and consequences of wind turbine wake effects arising from uncoordinated wind energy development, Nat. Energy 4 (2019) 26–34.
[2] X. Yang, F. Sotiropoulos, A review on the meandering of wind turbine wakes, Energies 12 (2019) 4725.
[3] D. Foti, Coherent vorticity dynamics and dissipation in a utility-scale wind turbine wake with uniform inflow, Theor. Appl. Mech. Lett. (2021) 100292.
[4] Z. Li, X. Yang, Large-eddy simulation on the similarity between wakes of wind turbines with different yaw angles, J Fluid Mech 921 (2021).
[5] F. Porté-Agel, M. Bastankhah, S. Shamsoddin, Wind-turbine and wind-farm flows: a review, Boundary Layer Meteorol 174 (2020) 1–59.
[6] P. Veers, K. Dykes, E. Lantz, et al., Grand challenges in the science of wind energy, Science 366 (2019) 6464.
[7] A. Platis, S.K. Siedersleben, J. Bange, et al., First in situ evidence of wakes in the far field behind offshore wind farms, Sci Rep 8 (1) (2018) 1–10.
[8] M.B. Christiansen, C.B. Hasager, Wake effects of large offshore wind farms identified from satellite sar, Remote Sens Environ 98 (2–3) (2005) 251–268.
[9] V. Pettas, M. Kretschmer, A. Clifton, et al., On the effects of inter-farm interactions at the offshore wind farm alpha ventus, Wind Energy Science (2021) 1–25.
[10] S. Frandsen, On the wind speed reduction in the center of large clusters of wind turbines, J. Wind Eng. Ind. Aerodyn. 39 (1–3) (1992) 251–265.
[11] D.W. Keith, J.F. DeCarolis, D.C. Denkenberger, et al., The influence of large-scale wind power on global climate, Proceedings of the National Academy of Sciences 101 (46) (2004) 16115–16120.
[12] P.A. Jiménez, J. Navarro, A.M. Palomares, et al., Mesoscale modeling of offshore wind turbine wakes at the wind farm resolving scale: a composite-based analysis with the weather research and forecasting model over horns rev, Wind Energy 18 (3) (2015) 559–566.
[13] A.C. Fitch, J.B. Olson, J.K. Lundquist, et al., Local and mesoscale impacts of wind farms as parameterized in a mesoscale nwp model, Mon. Weather Rev. 140 (2012) 3017–3038.
[14] Q. Wang, K. Luo, R. Yuan, et al., Wake and performance interference between adjacent wind farms: case study of xinjiang in china by means of mesoscale simulations, Energy 166 (2019) 1168–1180.
[15] O. Eriksson, Numerical computations of wakes behind wind farms, Institutionen för geovetenskaper, 2015 Ph.D. Thesis.
[16] H. Meng, S. Han, X. Yu, et al., Study on the wind-farm wake under neutral atmospheric condition, Int. J. Green Energy (2021) 1–9.
[17] X. Yang, M. Pakula, F. Sotiropoulos, Large-eddy simulation of a utility-scale wind farm in complex terrain, Appl. Energy 229 (2018) 767–777.
[18] K.L. Wu, F. Porté-Agel, Flow adjustment inside and around large finite-size wind farms, Energies 10 (12) (2017), doi:10.3390/en10122164.
[19] X. Yang, F. Sotiropoulos, R.J. Conzemius, et al., Large-eddy simulation of turbulent flow past wind turbines/farms: the virtual wind simulator (VWis), Wind Energy 18 (2015) 2025–2045.
[20] M. Germano, U. Piomelli, P. Moin, et al., A dynamic subgrid-scale eddy viscosity model, Physics of Fluids A: Fluid Dynamics 3 (1991) 1760–1765.
[21] L. Ge, F. Sotiropoulos, A numerical method for solving the 3D unsteady incompressible navier–Stokes equations in curvilinear domains with complex immersed boundaries, J. Comput. Phys. 225 (2007) 1782–1809.
[22] D. Knoll, D. Keyes, Jacobian-free newton-krylov methods: a survey of approaches and applications, J. Comput. Phys. 193 (2004) 357–397.
[23] Z. Li, X. Yang, Evaluation of actuator disk model relative to actuator surface model for predicting utility-scale wind turbine wakes, Energies 13 (2020), doi:10.3390/en13143574.
[24] M. Calaf, C. Meneveau, J. Meyers, Large eddy simulation study of fully developed wind-turbine array boundary layers, Physics of fluids 22 (2010) 015110.
[25] X. Yang, S. Kang, F. Sotiropoulos, Computational study and modeling of turbine spacing effects in infinite aligned wind farms, Physics of Fluids 24 (2012) 115107.
[26] C. Wu, X. Yang, Y. Zhu, On the design of potential turbine positions for physics-informed optimization of wind farm layout, Renew Energy 164 (2021) 1108–1120.